https://doi.org/10.5194/amt-2022-20
Preprint. Discussion started: 18 January 2022
© Author(s) 2022. CC BY 4.0 License.

Atmospheric Measurement Techniques
Discussions
Open Access

A Statistically Optimal Analysis of Systematic Differences between Aeolus HLOS Winds and NOAA's Global Forecast System

Hui Liu[1,2], Kevin Garrett[1], Kayo Ide[3], Ross N. Hoffman[1,2], and Katherine E. Lukens[1,2]

[1]NOAA/NESDIS/Center for Satellite Applications and Research (STAR), College Park, MD 20740, USA

[2]Cooperative Institute for Satellite Earth System Studies (CISESS), University of Maryland, College Park, MD 20740, USA

[3]University of Maryland, College Park, MD 20740, USA

Correspondence to: Kevin Garrett, NOAA/NESDIS/STAR, 5830 University Research Ct, College Park, MD 20740, USA. Email: kevin.garrett@noaa.gov. Phone: (301) 683-3641.

Coauthor contact information:
Hui Liu: Hui.Liu@noaa.gov, ORCID 0000-0002-7959-0984.
Kevin Garrett: : kevin.garrett@noaa.gov, ORCID 0000-0002-7444-4363.
Kayo Ide: Kayo.Ide@noaa.gov, ORCID 0000-0001-5789-9326.
Ross N. Hoffman: Ross.N.Hoffman@noaa.gov, ORCID 0000-0002-4962-9438.
Katherine E. Lukens: Katherine.Lukens@noaa.gov.

https://doi.org/10.5194/amt-2022-20
Preprint. Discussion started: 18 January 2022
© Author(s) 2022. CC BY 4.0 License.

Key Points

- There are speed-dependent systematic differences in the Aeolus M1-bias corrected Level-2B HLOS winds compared to short-term (6-h) FV3GFS forecasts.
- The total least squares (TLS) regression provides a statistically optimal analysis of the differences.
- A bias correction based on the TLS bias analysis proposed here is tested in a companion paper to optimize Aeolus wind assimilation and thus the impact of Aeolus winds on global NWP forecasts.

https://doi.org/10.5194/amt-2022-20
Preprint. Discussion started: 18 January 2022
© Author(s) 2022. CC BY 4.0 License.

Atmospheric Measurement Techniques Discussions
Open Access

Abstract

The European Space Agency Aeolus mission launched the first of its kind spaceborne Doppler wind lidar in August 2018. To optimize assimilation of the Aeolus Level-2B (L2B) Horizontal Line-of-Sight (HLOS) winds, systematic differences (referred as biases hereafter) between the observations and numerical weather prediction (NWP) background winds should be removed. Total least squares (TLS) regression is used to estimate speed-dependent biases between Aeolus HLOS winds (L2B10) and the National Oceanic and Atmospheric Administration (NOAA) Finite-Volume Cubed-Sphere Global Forecast System (FV3GFS) 6-h forecast winds. Unlike ordinary least squares regression, TLS regression optimally accounts for random errors in both predictors and predictands. Large well-defined, speed-dependent biases are found particularly in the lower stratosphere and troposphere of the tropics and Southern Hemisphere. These large biases should be corrected to increase the forecast impact of Aeolus data assimilated into global NWP systems.

Key words: Aeolus winds, Doppler wind lidar, total least squares, bias correction

https://doi.org/10.5194/amt-2022-20
Preprint. Discussion started: 18 January 2022
© Author(s) 2022. CC BY 4.0 License.

1 Introduction

The space-borne Doppler wind lidar on board the European Space Agency (ESA) Aeolus mission measures both Rayleigh (i.e., molecular) and Mie (i.e., clouds and aerosols) backscatter to derive wind profiles along the sensor's Horizontal Line of Sight (HLOS) throughout the troposphere and lower stratosphere [Straume-Lindner, 2018, Straume et al., 2020]. The Aeolus HLOS Level-2B (L2B) winds have demonstrated positive impacts on global weather forecasts [Rennie et al., 2021; Cress, 2020; Garrett et al., 2020, 2021].

To optimize the positive impact of Aeolus winds on weather forecasts, large systematic differences (referred to as biases hereafter) between Aeolus winds and numerical weather prediction (NWP) model background winds should be corrected [Daley, 1991]. Therefore, it is important to identify potential biases between Aeolus winds and their NWP model background counterparts [Liu et al., 2020, 2021]. The biases may come from both NWP models and Aeolus winds. First, current operational global NWP models still have larger errors or uncertainty in regions where conventional observations are sparse or absent, and these errors include bias components as the NWP models evolve towards their own climatology in the absence of observations. For example, the backgrounds from the ECMWF model (https://www.ecmwf.int/en/forecasts) and the NOAA Finite-Volume Cubed-Sphere Global Forecast System (FV3GFS) model (https://www.gfdl.noaa.gov/fv3/) show large systematic differences in the zonal winds in the troposphere and lower stratosphere of the tropics, the Southern Hemisphere (SH), and north of 70° N, with maxima on the order of 2.0, -0.5, and 0.5 m/s, respectively (see Figure 1).

https://doi.org/10.5194/amt-2022-20
Preprint. Discussion started: 18 January 2022
© Author(s) 2022. CC BY 4.0 License.

Secondly, although corrections to several substantial bias sources in the Aeolus L2B winds have been implemented, including corrections to the dark current signal anomalies of single pixels (so-called hot pixels) on the Accumulation-Charge-Coupled Devices (ACCDs), linear drift in the illumination of the Rayleigh/Mie spectrometers, and the telescope M1 mirror temperature variations [Reitebuch et al., 2020; Weiler et al., 2021], uncorrected biases due to potential calibration issues might remain in Aeolus L2B winds and may contribute to potential biases between Aeolus and the NWP background winds. The residual biases may lead to sub-optimal assimilation of Aeolus winds in NWP systems. In addition, the Aeolus L2B winds might be biased towards the ECMWF model, as the M1 bias correction makes use of ECMWF 6-hour forecasts [Rennie et al., 2021], which might also lead to sub-optimal assimilation of Aeolus winds in other NWP systems.

Using ordinary least squares (OLS) to identify and estimate the speed-dependent biases in the innovations of Aeolus minus NWP background winds (O-B) is subject to contamination from random errors in Aeolus and/or NWP background winds [Frost and Thompson, 2000], since OLS assumes no errors in the predictor or independent variable, which in this case would be either the Aeolus winds, the NWP background winds, or a combination of the two. In contrast, total least squares (TLS) regression takes account of errors in both dependent and independent variables and generates a statistically optimal analysis of the biases [Deming, 1943; Ripley and Thompson, 1987; Markovsky and Van Huffel, 2007]. For the case of Aeolus and NWP background winds, the use of linear TLS regression [Ripley and Thompson, 1987] finds a best fit line that is an estimate of the true (assumed linear) relationship between Aeolus and NWP background winds.

https://doi.org/10.5194/amt-2022-20
Preprint. Discussion started: 18 January 2022
© Author(s) 2022. CC BY 4.0 License.

In this study, the TLS regression approach is used to identify and estimate potential biases between the Aeolus HLOS winds (L2B10) and the NOAA FV3GFS background winds. The suboptimality of OLS bias estimates is demonstrated by comparison to the TLS bias estimates. A bias correction based on the TLS bias analysis is proposed for the innovations of Aeolus minus FV3GFS winds in order to optimize Aeolus wind assimilation with the FV3GFS model and thus improve the impact of Aeolus winds on FV3GFS forecasts.

Section 0 describes the Aeolus L2B and FV3GFS background winds, the TLS bias analysis method, and the estimation of the ratio of error variances of Aeolus winds to FV3GFS background winds used in the TLS regression. Section 3 describes the variations of the TLS bias estimates with height, latitude, and wind speed. Section 4 demonstrates the substantial differences between the TLS and OLS bias estimates. Section 5 proposes a TLS bias correction for the O-B innovations. Finally, Section 6 presents a summary of findings and conclusions. Throughout this article, we will refer to the Aeolus and FV3GFS HLOS winds as the Aeolus and FV3GFS winds, respectively. In discussions of winds that are not HLOS winds we will use terms like *u*-wind, *v*-wind, or wind vector.

2 Data and Methodology

2.1 Aeolus L2B and FV3GFS background wind data

The Aeolus L2B clear-sky Rayleigh winds and cloudy-sky Mie winds are examined for the period 1-7 September 2019. This one-week period provides a sufficient sample to estimate the biases. The Aeolus winds were obtained from the Aeolus dataset (L2B10) re-processed by ESA [Rennie et al., 2021, Weiler et al., 2021]. The reprocessing includes the M1 bias correction,

https://doi.org/10.5194/amt-2022-20
Preprint. Discussion started: 18 January 2022
© Author(s) 2022. CC BY 4.0 License.

which removes most of the globally and vertically averaged biases of Rayleigh and Mie winds [Weiler et al., 2021]. The Aeolus winds are reported at a standard set of vertical layers [de Kloe, 2019, 2020]. This study examines Aeolus Mie and Rayleigh winds within height ranges of 0-16 km and 3-22 km, respectively. These height ranges include almost all Aeolus wind observations. The height is defined relative to the EGM96 geoid for the L2B winds [Tan et al. 2008].

Similar Aeolus data quality control procedures as recommended by ESA and ECMWF [Rennie et al., 2021] were implemented to reject the following observations: HLOS L2B confidence flag "invalid"; Rayleigh winds at layers below 850 hPa, L2B uncertainties greater than 12 m/s, accumulation lengths less than 60 km, and atmospheric pressure within 20 hPa of topographic surface pressure; Mie winds with L2B uncertainties greater than 5 m/s and accumulation lengths less than 5 km.

The winds from Aeolus and collocated FV3GFS backgrounds are obtained from a data assimilation experiment (hereafter the BASE experiment) where the Aeolus winds are monitored and the Aeolus wind observation operator (H_i) is applied to the FV3GFS background ($\mathbf{x}^b$) to obtain the value of FV3GFS background wind ($y_i^b = H_i(\mathbf{x}^b)$) corresponding to each Aeolus observation (y_i^o). This experiment employs the FV3GFS data assimilation system, called Global Statistical Interpolation [GSI, Kleist et al. 2009], configured for the 4DEnVar algorithm with 64 vertical levels, and horizontal resolutions of C384 (~25 km) for the deterministic analysis and forecast and C192 (~50 km) for the 80 ensemble members [Wang and Lei, 2014].

When examining Aeolus wind statistics, we stratify the Aeolus data by orbital phase, either ascending when the spacecraft is moving northward or descending when the spacecraft is moving southward. The vertical and daily variations of global horizontal means and standard

https://doi.org/10.5194/amt-2022-20
Preprint. Discussion started: 18 January 2022
© Author(s) 2022. CC BY 4.0 License.

deviations of the innovations of Mie winds minus FV3GFS background winds are consistent throughout the period (Figs. 2 and 3). For Mie winds in ascending orbits, the biases are positive above 6 km and negative below 6 km, as large as +1.8 m/s and -0.5 m/s, respectively. The biases are smaller and positive at most levels in the descending orbits. The standard deviations are smallest (about 4 m/s) from 2 to 8 km elevation and increase to only about 5 m/s at the highest levels. For Rayleigh winds in descending orbits, the biases are as positive as +1.2 m/s above 10 km, and as negative as -1.2 m/s below 8 km. The positive biases in ascending orbits are smaller. The standard deviations are smallest (again about 4 m/s) from 6 to 12 km elevation and increase to about 7 m/s at the highest levels. The results indicate that the biases vary substantially with height for both Mie and Rayleigh winds, the standard deviations vary from 4 m/s to somewhat larger values at higher elevations, and that both mean and standard deviations remain stable in time throughout the period.

The mean differences of Mie and Rayleigh winds minus FV3GFS winds vary considerably with latitude (Figure 4). Mie winds have biases as large as +1.5 m/s in the upper troposphere and Rayleigh winds have biases as large as +2.0 m/s in the tropical upper troposphere. Both Mie and Rayleigh winds show negative biases as large as -1.0 m/s in the lowest layers.

2.2 TLS Linear Regression

In this section, we review the TLS regression method [Ripley and Thompson, 1987] in the context of estimating potential speed-dependent biases between Aeolus winds and FV3GFS background winds. The TLS estimate for each collocated pair of Aeolus and FV3GFS winds (y_i^o, y_i^b) is defined by

https://doi.org/10.5194/amt-2022-20
Preprint. Discussion started: 18 January 2022
© Author(s) 2022. CC BY 4.0 License.

$$y_i^o = \hat{y}_i^o + \varepsilon_i^o \quad \text{and} \quad y_i^b = \hat{y}_i^b + \varepsilon_i^b \qquad (i = 1, N) \qquad (1)$$

where $\hat{y}_i^o$ and $\hat{y}_i^b$ are the TLS estimates of the true Aeolus and FV3GFS winds, and ε_i^o and ε_i^b are random errors, and N is the number of Aeolus/FV3GFS collocations in the sample. The sample might be defined by a vertical layer or a latitude band. In OLS regression, since it is assumed that there are no errors in the predictor, the predictor can be used directly to estimate the predictand. The situation is a little more complicated in TLS regression where ($\hat{y}_i^b$, $\hat{y}_i^o$), the most probable true state, is the point on the regression line that is closest in a statistical sense to the point (y_i^b, y_i^o).

Here we assume that ε_i^o and ε_i^b are independent and that the random error variance ratio $\delta = (\sigma^o/\sigma^b)^2 = \mathrm{E}[\varepsilon_i^o \varepsilon_i^o] / \mathrm{E}[\varepsilon_i^b \varepsilon_i^b]$ is known. Also, we assume the true relationship between the Aeolus and FV3GFS winds is described by a linear function:

$$\hat{y}_i^o = c_0 + c_1 \hat{y}_i^b \qquad (i = 1, N) \qquad (2)$$

where c_0 is an offset or constant bias and c_1 is a speed-dependent bias coefficient.

The TLS regression finds an optimal estimate of the $\hat{y}_i^b$, c_0 and c_1 by minimizing the cost function

$$\mathrm{J} = \sum_{i=1}^{N} \left((\varepsilon_i^o/\sigma^o)^2 + \left(\varepsilon_i^b/\sigma^b\right)^2 \right)$$

$$= \frac{1}{(\sigma^o)^2} \sum_{i=1}^{N} \left(\left(y_i^o - c_0 - c_1 \hat{y}_i^b\right)^2 + \delta\left(y_i^b - \hat{y}_i^b\right)^2 \right)$$

To determine the $\hat{y}_i^b$, set the derivative of J with respect to $\hat{y}_i^b$ to zero, to obtain

$$\hat{y}_i^b = (c_1(y_i^o - c_0) + \delta y_i^b) / (c_1^2 + \delta) \qquad (i = 1, N) \qquad (3)$$

https://doi.org/10.5194/amt-2022-20
Preprint. Discussion started: 18 January 2022
© Author(s) 2022. CC BY 4.0 License.

Eq. (3) thereby reduces the problem to a minimization in terms of c_0 and c_1. A similar equation holds even if the error variances vary with *i*, but then there is no closed form solution for c_0 and c_1, as there is in the current case, which is known as the Deming problem [Ripley and Thompson, 1987]. When the coefficients c_0 and c_1 are obtained, the TLS estimate for the new or within-sample observation is given by Eq. (3). Finally, the estimate of the bias for the *k*th observation, either for a new or within-sample observation, is given by

$$\hat{d}_k = \hat{y}_k^o - \hat{y}_k^b = c_0 + (c_1 - 1)\hat{y}_k^b \quad (4)$$

We will refer to c_0 and $(c_1 - 1)$ as the constant and speed-dependent bias coefficients, respectively, hereafter.

Note that the error variance ratio δ is a crucial parameter in the TLS bias analysis. If $\sigma^o = 0$ or $\sigma^b = 0$, then the TLS solution is equivalent to the OLS regression of the O-B on the Aeolus winds or on the FV3GFS winds, respectively.

2.3 Estimation of the random error variance ratio

The random error variance ratio $\delta = (\sigma^o/\sigma^b)^2$ used in the TLS bias analysis is estimated from the O-B innovations from the BASE experiment using the Hollingsworth-Lonnberg (HL) method [Hollingsworth and Lonnberg, 1986]. It is assumed that there is no correlation between the random errors in Aeolus and FV3GFS winds and no horizontal correlation in the random errors in Aeolus winds at 90 km distance and beyond. For more details, see Hollingsworth and Lonnberg [1986] and Garrett et al. [2021].

The random error variance ratio δ is estimated at the middle height of each vertical range bin using the Aeolus samples for 1-7 September 2019, separately for Mie and Rayleigh winds.

https://doi.org/10.5194/amt-2022-20
Preprint. Discussion started: 18 January 2022
© Author(s) 2022. CC BY 4.0 License.

Figure 5 shows that the vertical profiles of the square root of δ varies in the range of 1.2-1.6 and 2-3 for Mie winds versus FV3GFS winds and Rayleigh winds versus FV3GFS winds, respectively.

3 The TLS Bias Estimates

The statistical relationship between Aeolus and FV3GFS winds is illustrated by the density plots of collocated Aeolus and FV3GFS winds in a single layer shown in Figure 6. There is a strong correlation of 0.93 between Mie and FV3GFS winds, and of 0.94 between Rayleigh and FV3GFS winds. The TLS analyses of the FV3GFS winds versus Aeolus winds indicate that the innovations (Aeolus minus FV3GFS winds) are positive and increase with wind speed. In terms of Eq. (4), for Figure 6a, the innovation solution is 0.53 m/s + 0.06 times the background solution, while for Figure 6b, the innovation solution is 1.04 m/s + 0.04 times the background solution.

3.1 Variation of Biases with Height

The variation of the TLS solution with height and orbital phase is described here. The TLS samples are over all latitudes. The vertical distribution of the TLS constant and speed-dependent bias analysis coefficients for the innovation in terms of the background in Eq. (4) is shown in Figure 7. The speed-dependent bias coefficient $(c_1 - 1)$ varies substantially with height and orbital phase. For Mie winds, the coefficient is quite large at most heights, ranging from 3 to 6%, with maxima at 3 km and 12-16 km. The coefficient for Rayleigh winds is smaller and ranges from 1 to 3% in ascending orbits and 1 to 5% in descending orbits, with maxima around the 3.5 and 16 km.

© Author(s) 2022. CC BY 4.0 License.

The constant bias coefficient c_0 for both Mie and Rayleigh winds also shows large variations on height and orbit with its value as large as +/- 1.0 m/s. In general, the constant bias coefficient is positive in upper layers and negative in layers close to the Earth surface, consistent with the patterns seen in the global horizontal average of innovations in Figures 2 and 3.

The vertical distribution of the average TLS bias estimates as function of Aeolus wind is shown in Figure 8. The average TLS biases vary substantially with height. Since the TLS biases are in part dependent on speed, at most heights the biases increase substantially as the magnitude of Aeolus wind speed increases. The biases at high Aeolus wind speeds are considerably larger for Mie winds than for Rayleigh winds, as large as +2.5 m/s and -2.0 m/s for Mie winds, and +1.5 m/s and -2.0 m/s for Rayleigh winds. There are clear speed-dependent biases in the vertical average of these biases (Figure 9). The results suggest that both vertically varying and vertically averaged speed-dependent biases remain in the Aeolus winds (L2B10).

3.2 Variation of Biases with Latitude

The variation of the TLS solution with latitude and orbital phase is described here. The TLS samples are over all heights for 10-degree latitude bands. In general, the coefficients obtained are large and vary considerably with latitude and orbital phase, with maxima found in the tropics (Figure 10). For example, the speed-dependent bias coefficient $(c_1 - 1)$ for Mie winds in the tropics can be quite large, ranging from 0% to a maximum of 11%. The coefficient $(c_1 - 1)$ is smaller for Rayleigh winds, ranging from -1% to 5%, with maxima found in the tropics and at northern high latitudes. The constant bias coefficient c_0 for Mie winds also varies considerably with latitude and orbit, ranging from -1.0 m/s to +1.6 m/s. The coefficient c_0 is smaller for Rayleigh winds.

https://doi.org/10.5194/amt-2022-20
Preprint. Discussion started: 18 January 2022
© Author(s) 2022. CC BY 4.0 License.

The latitudinal distribution of the average TLS bias as a function of Aeolus wind is shown in Figure 11. For Mie winds, the average TLS bias increases considerably at most latitudes as the magnitude of Aeolus wind speed increases, particularly in the tropics and SH, with maxima of about +/-2.5 m/s. For Rayleigh winds, the average biases are much smaller and are consistent with the fact that the M1 bias correction removes most globally and vertically averaged biases of Rayleigh winds [Weiler et al., 2021].

3.3 Discussion

The results presented in this section indicate that the speed-dependent bias coefficient is quite large, with $(c_1 - 1)$ reaching up to ~10% and 5% for Mie and Rayleigh winds, respectively, particularly in the lower stratosphere and lower troposphere of the tropics. This suggests that there exist large speed-dependent biases in FV3GFS background winds and/or in the Aeolus winds. Given that there exist large uncertainties in the FV3GFS (and ECMWF) background winds in the tropics (see Figure 1), it is likely that the FV3GFS may be a significant source of the large biases and this will require further investigation. In any case, these large speed-dependent biases should be corrected to optimize Aeolus wind assimilation and the impact of Aeolus winds on NWP forecasts.

4 Comparison to OLS Regressions

As a comparison to the TLS bias estimate results, we conducted parallel OLS regressions using three different predictors of the biases in O-B. These predictors are the FV3GFS winds, the Aeolus winds, and their average. The first two of these OLS regressions are equivalent to OLS regressing Aeolus on FV3GFS winds and OLS regressing FV3GFS on Aeolus winds. As examples, the regression lines of these two cases are added to Figure 6. The TLS speed-dependent coefficient $(c_1 - 1)$ (in Eq. 4) = 6% and 4% for Mie and Rayleigh winds, respectively. However, the OLS regression of Aeolus winds on FV3GFS winds produces considerably smaller bias estimates, with $(c_1 - 1)$ estimated as 1% and 2% for Mie and Rayleigh winds, respectively; thus, this OLS regression considerably underestimates the biases.

On the other hand, the OLS regression of the FV3GFS winds on Aeolus winds exhibits much larger bias estimates relative to the TLS bias analysis, with $(c_1 - 1)$ estimated as 18% and 15% for Mie and Rayleigh winds, respectively. This indicates that the speed-dependent biases are considerably overestimated by the OLS regression on Aeolus winds.

The vertical distributions of the average biases as a function of Aeolus winds are shown in Figure 12 for the descending orbits for three methods: The top panels are for OLS regression using FV3GFS winds as a predictor, the middle panels, which repeat the bottom two panels of Figure 8 are for TLS regression, and the bottom panels are for OLS regression using the average of FV3GFS and Aeolus as a predictor (bottom). The average bias estimates in the top panels are about 0.5-1.0 m/s smaller in magnitude in most layers than the middle panels. This confirms that, on average, the biases are considerably underestimated by OLS regression using FV3GFS winds as a predictor.

The average biases in the bottom panel are about 0.5-1.5 m/s in magnitude larger than the middle panel in most layers, particularly for Rayleigh winds, indicating the biases are overestimated by OLS regression using the average of Aeolus and FV3GFS winds as a predictor. The bias estimates of OLS regression using Aeolus winds only as a predictor (not shown) are even larger (than the bottom panel).

https://doi.org/10.5194/amt-2022-20
Preprint. Discussion started: 18 January 2022
© Author(s) 2022. CC BY 4.0 License.
Atmospheric Measurement Techniques Discussions

5 A TLS Bias Correction

In this section, a TLS bias correction for O-B is proposed to optimize Aeolus wind data assimilation. For each assimilation cycle, the bias coefficients are computed by TLS regression for the O-B in the week before the cycle (i.e., for the previous 28 cycles). One week provides a large enough sample for the regression. As shown by Ripley and Thompson [1987], the TLS solution only involves solving a quadratic equation with coefficients given by sample sums. Therefore, an efficient approach is to calculate and save these sums for every cycle and accumulate them over the 28 cycles. Because the findings in this study show substantial variation of the bias coefficients with latitude, vertical layer, and orbital phase, the bias coefficients are calculated from the winds in 19 discrete bins of latitude (centered every 10° between 90° S to 90° N) for each vertical range/layer and for ascending and descending orbits separately. For each of the O-B innovations in the assimilation cycle, values of c_0 and c_1 are linearly interpolated to the latitude of the Aeolus observation. Subsequently, the TLS estimated bias, calculated using Eq. (4), is subtracted from the O-B. Note that the bias correction is determined by the TLS analysis solution for $\hat{y}_k^b$ that in turn is determined from the observation and background wind, y_k^o and y_k^b, following Eq. (3).

The proposed scheme is applied to the O-B innovations of the BASE experiment. The vertical distribution of the average remaining biases as a function of Aeolus wind is shown in Figure 13, which is in the same format and for the same sample of observations as Figure 8. A comparison of these two figures reveals that most of the biases are removed by the proposed TLS bias correction. The latitudinal variations of the biases are also corrected (Figure 14). In addition, the biases in the vertical average are also mostly removed, as shown in Figure 9.

https://doi.org/10.5194/amt-2022-20
Preprint. Discussion started: 18 January 2022
© Author(s) 2022. CC BY 4.0 License.
Atmospheric Measurement Techniques Discussions

6 Summary and Conclusions

In this study a TLS regression is used to optimally estimate speed-dependent biases between Aeolus L2B Horizontal Line-of-Sight winds and short-term (6-h) forecasts of NOAA's FV3GFS. The winds for 1-7 September 2019 are analyzed. Clear speed-dependent biases for both Mie and Rayleigh winds are found, particularly in the lower troposphere and stratosphere of the tropics and Southern Hemisphere. The largest biases are about 10% and 5% of FV3GFS wind speed, as large as +/- 2.5 m/s and +/- 1.5 m/s at high FV3GFS wind speed, for Mie and Rayleigh winds, respectively.

It is found that the biases are considerably underestimated by the OLS regression of the innovations of Aeolus winds minus FV3GFS background winds on FV3GFS winds; but are overestimated by the OLS regression, both on Aeolus winds only, and on the average of Aeolus and FV3GFS winds.

The biases should be fully corrected to optimize Aeolus wind assimilation and to improve the impact of Aeolus winds on FV3GFS global forecasts. The proposed TLS bias correction can remove most of the biases before assimilation. In a companion paper, Garrett et al. [2021] demonstrate that the application of this TLS bias correction to the Aeolus minus FV3GFS background (O-B) winds considerably enhances the positive impact of Aeolus winds on NOAA FV3GFS global and tropical cyclone forecasts. It is expected that the application of this additional bias correction to the O-B innovations of Aeolus winds can improve and enhance Aeolus data impacts on the analysis and forecast skill of other NWP systems as well.

Note that the proposed TLS approach presented here might be applied to other types of observations that have errors typically characterized as a percentage of the observed value,

https://doi.org/10.5194/amt-2022-20
Preprint. Discussion started: 18 January 2022
© Author(s) 2022. CC BY 4.0 License.
Atmospheric Measurement Techniques Discussions

including quantities related to the concentrations or mass fractions of chemical species or hydrometeors, or quantities like radio occultation refractivity and bending angle.

Acknowledgments

This work was supported by the NOAA/NESDIS Office of Projects, Planning, and Acquisition (OPPA) Technology Maturation Program (TMP), managed by Patricia Weir and Dr. Nai-Yu Wang, through the Cooperative Institute for Satellites and Earth System Studies (CISESS) at the University of Maryland (Grant NA14NES4320003 and NA19NES4320002). The authors would like to acknowledge Dr. Michael Rennie (ECMWF) and Dr. Lars Isaksen (KNMI) for their comments and suggestions on the assimilation of Aeolus observations, and Dr. William McCarty with NASA/GMAO for providing earlier versions of the GSI with Aeolus ingest and observation operator capability. The Aeolus L2B BUFR data were provided by ECMWF. The scientific results and conclusions, as well as any views or opinions expressed herein, are those of the author(s) and do not necessarily reflect those of NOAA or the U.S. Department of Commerce.

7 References

Cress, A.: Validation and impact assessment of Aeolus observations in the DWD modeling system. Status report'. *Aeolus NWP Impacts Working Meeting,* Virtual, 2020. Available at: https://www.aeolus.esa.int/confluence/display/CALVAL/Aeolus+NWP+impact+working+meeting+2?preview=/12354328/12354463/5_DWD_acress_aeolus_20200617.pdf.

© Author(s) 2022. CC BY 4.0 License.

Daley R.: Atmospheric data analysis. Cambridge University Press, Cambridge, 457 pp., ISBN-13 978-0521458252, 1991

de Kloe, J. and Coauthors: Aeolus Data Innovation Science Cluster DISC ADM-Aeolus Level-2B/2C Processor Input/Output Data Definitions Interface Control Document. *Tech. rep.*, KNMI, Aeolus, DISC, REF: AED-SD-ECMWF-L2B-037, 2020. Available at: https://earth.esa.int/eogateway/documents/20142/37627/Aeolus-L2B-2C-Input-Output-DD-ICD.pdf.

Deming, W. E.: Statistical adjustment of data, Wiley, NY (Dover Publications edition, 1985). ISBN 0-486-64685-8, 1943.

Frost, C. and Thompson S.: Correcting for regression dilution bias: comparison of methods for a single predictor variable, Journal of the Royal Statistical Society, Series A 163: 173–190. https://doi.org/10.1111/1467-985X.00164, 2020.

Garrett, K., Liu, H., Ide, K., Lukens, K., and Cucurull, L.: Updates to Aeolus Impact Assessment on NOAA global NWP. 2nd ESA Aeolus Cal/Val and Science Workshop, Nov 2-6, 2020. Available at: https://www.dropbox.com/s/cd0r1gz7t77gq0g/Kevin_Garrett_Oral_Evaluation_of_Aeolus.pptx?dl=0.

Garrett K., H. Liu, K. Ide, R. N. Hoffman, and K. E. Lukens: Optimization and Impact Assessment of Aeolus HLOS Wind Data Assimilation in NOAA's Global Forecast System, *Q. J. R. Meteorol. Soc.*, submitted, manuscript QJ-21-0307, 2022.

© Author(s) 2022. CC BY 4.0 License.

Hollingsworth, A. and Lonnberg, P.: The statistical structure of short-range forecast errors as determined from radiosonde data. Part I: The wind field. Tellus, 38A, Issue 2, p111-136. https://doi.org/10.3402/tellusa.v38i2.11707, 1986

Kleist, D. T. and Coauthors: Introduction of the GSI into the NCEP Global Data Assimilation System. *Wea. Forecasting*, **24**, 1691–1705, https://doi.org/10.1175/2009WAF2222201.1, 2009.

Liu, H., Garrett, K. Ide, K., Hoffman, R. N., and Lukens, K. E.: Bias correction and Error Specification of Aeolus Winds for NOAA Global Data Assimilation System. 2nd ESA Aeolus CAL/VAL and Science Workshop, Nov 2-6, 2020. Available at: https://www.dropbox.com/s/f518n7n8ouhgwhy/Hui_LIU_Flash_Evaluation_update.pdf?dl=0.

Liu H., K. Garrett, K. Ide, R. Hoffman, and K Lukens: Impact Assessment of Aeolus Winds on NOAA Global Forecast, European Geophysical Union general assembly, 19-30 Apr 2021. Available at: https://meetingorganizer.copernicus.org/EGU21/session/40837.

Markovsky I. and Van Huffel S.: Overview of total least squares methods. Signal Processing, vol. 87, pp. 2283–2302. doi: 10.1016/j.sigpro.2007.04.004, 2007.

Reitebuch, O., Bracci, F., and Lux, O.: Assessment of the Aeolus performance and bias correction - results from the Aeolus DISC. 2nd Aeolus Cal/Val Workshop, Nov. 2020. Available at: https://www.dropbox.com/s/m3kjp540otwm17l/Oliver_Reitebuch_Oral_Assessment-Aeolus-DISC.pdf?dl=0.

https://doi.org/10.5194/amt-2022-20
Preprint. Discussion started: 18 January 2022
© Author(s) 2022. CC BY 4.0 License.

Rennie, M. P., Isaksen, L., Weiler, F., de Kloe, J., Kanitz, T. and Reitebuch, O.: The impact of Aeolus wind retrievals on ECMWF global weather forecasts, *Q. J. R. Meteorol. Soc.*, pp. 1–32, doi:10.1002/qj.4142, 2021.

Ripley, B. D. and Thompson M.: Regression techniques for the detection of analytical bias, Analyst, 112, 377-383. doi: 10.1039/AN987120037, 1987.

Straume-Lindner, A. G.: Aeolus Sensor and Product Description'. *Tech. rep.*, European Space Agency - European Space Research and Technology Centre, The Netherlands. REF: AE-SU-ESA-GS-000. Available at: https://earth.esa.int/eogateway/documents/20142/37627/Aeolus-Sensor-and-Product-Description.pdf, 2018.

Straume, A.G. and coauthors: ESA's Space-Based Doppler Wind Lidar Mission Aeolus First Wind and Aerosol Product Assessment Results. Edited by D. Liu, Y. Wang, Y. Wu, B. Gross, and F. Moshary. EPJ Web of Conferences 237: 01007, https://doi.org/10.1051/epjconf/202023701007, 2020.

Tan, D. G. H. and others: The ADM-Aeolus wind retrieval algorithms, Tellus A, 60, 191-205. doi:10.1111/j.1600-0870.2007.00285.x, 2008.

Wang, X. and Lei, T.: GSI-Based Four-Dimensional Ensemble–Variational (4DEnsVar) Data Assimilation: Formulation and Single-Resolution Experiments with Real Data for NCEP Global Forecast System. *Mon. Wea. Rev.*, **142**, 3303–3325, https://doi.org/10.1175/MWR-D-13-00303.1, 2014.

https://doi.org/10.5194/amt-2022-20
Preprint. Discussion started: 18 January 2022
© Author(s) 2022. CC BY 4.0 License.

Weiler F. M. Rennie, T. Kanitz, L. Isaksen, E. Checa, Jos de Kloe, O. Reitebuch: Correction of wind bias for the lidar on-board Aeolus using telescope temperatures, *Atmos. Meas. Tech.* doi: 10.5194/amt-2021-171, 2021.

https://doi.org/10.5194/amt-2022-20
Preprint. Discussion started: 18 January 2022
© Author(s) 2022. CC BY 4.0 License.

8 Figures

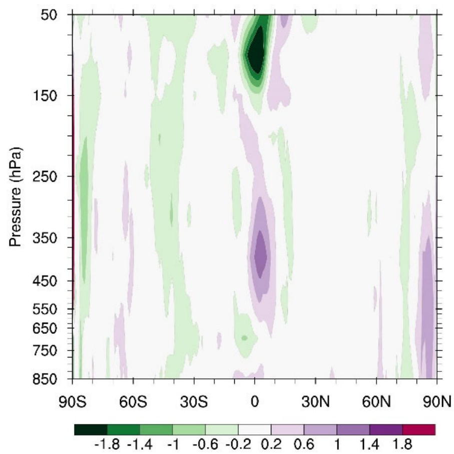

Figure 1. Latitudinal and height distributions of zonal mean difference of ECMWF minus FV3GFS background zonal wind (m/s) for 1-7 September 2019.

https://doi.org/10.5194/amt-2022-20
Preprint. Discussion started: 18 January 2022
© Author(s) 2022. CC BY 4.0 License.
Atmospheric Measurement Techniques
Discussions

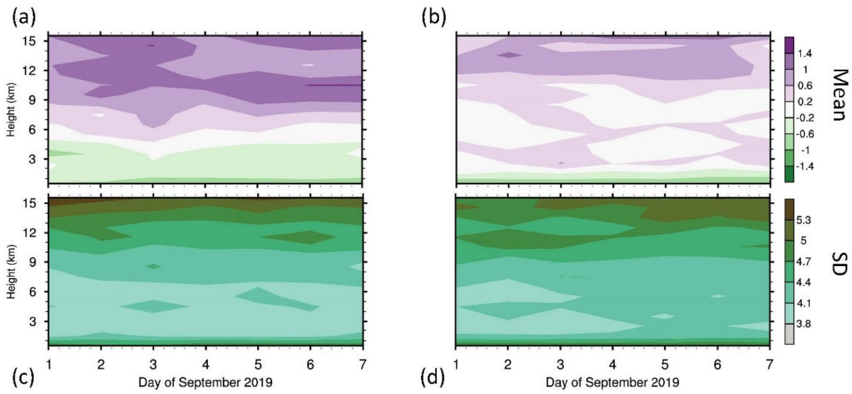

Figure 2. Vertical and daily variations of global horizontal means (a, b) and standard deviations (c, d) of the innovations of Mie winds minus FV3GFS background winds (m/s) in ascending (a, c) and descending (b, d) orbits.

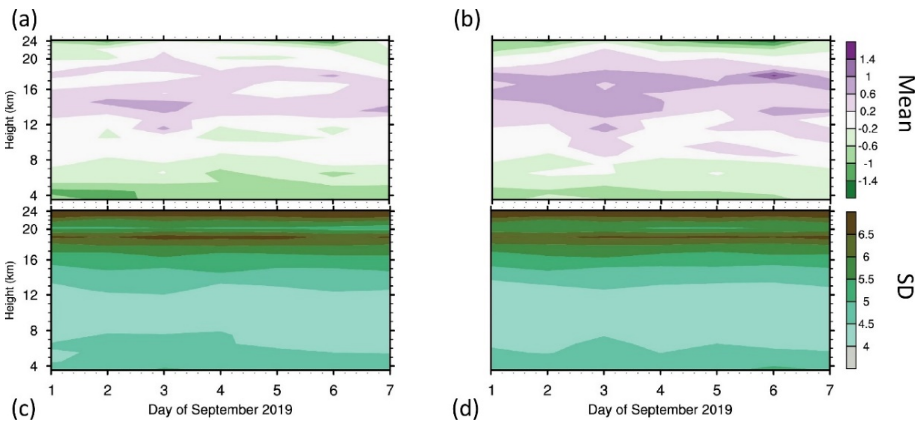

Figure 3. As in Fig. 2 but for Rayleigh winds.

https://doi.org/10.5194/amt-2022-20
Preprint. Discussion started: 18 January 2022
© Author(s) 2022. CC BY 4.0 License.

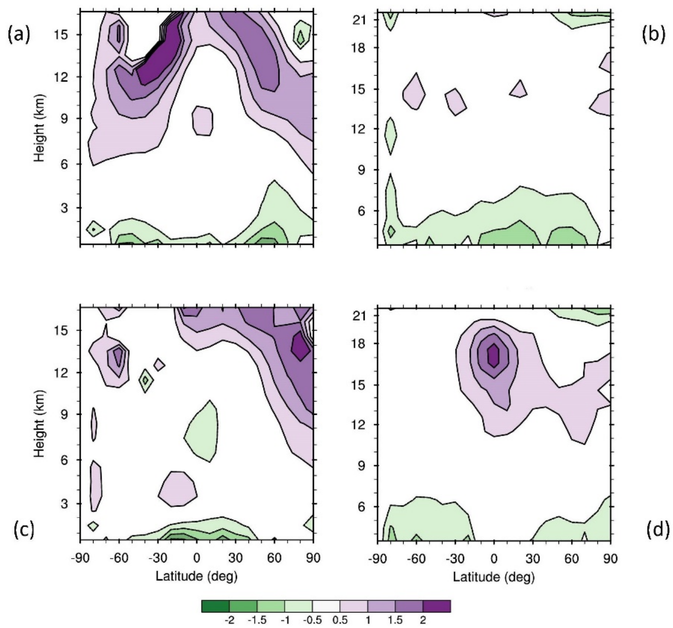

Figure 4. Latitudinal and height distributions of mean differences (color scale, m/s) of Mie minus FV3GFS winds (a, c) and Rayleigh minus FV3GFS winds (b, d) in ascending (a, b) and descending (c, d) orbits for 1-7 September 2019.

https://doi.org/10.5194/amt-2022-20
Preprint. Discussion started: 18 January 2022
© Author(s) 2022. CC BY 4.0 License.

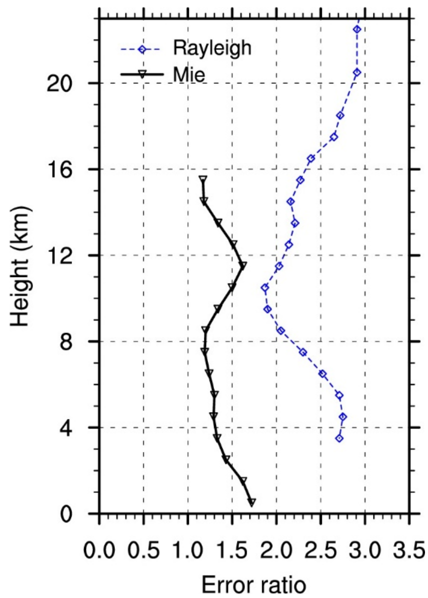

Figure 5. Vertical variation of the square root of the ratio of random error variance in Aeolus winds versus FV3GFS background winds for Mie (solid black) and Rayleigh (dashed blue) winds. Results are based on global O-B innovations of Aeolus minus FV3GFS winds from the Aeolus BASE experiment using Hollingsworth-Lonnberg method. The symbols are plotted at averaged height in each vertical layer.

Atmospheric Measurement Techniques Discussions

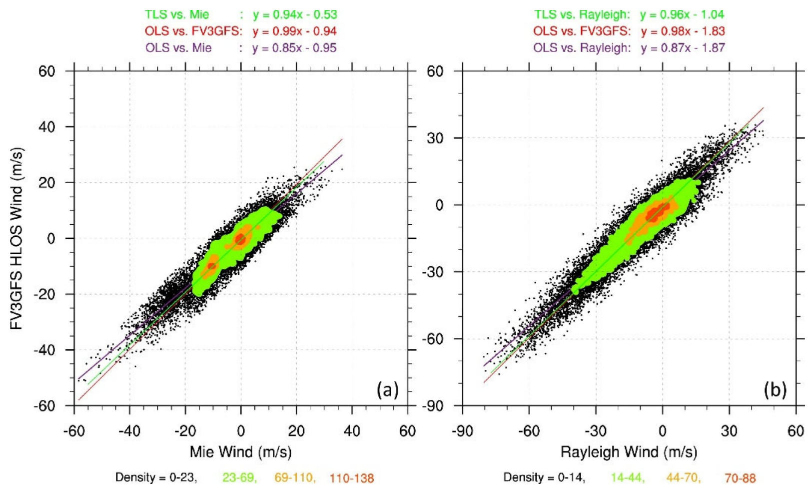

Figure 6. Density plots of global collocated Mie and FV3GFS winds at ~3.5 km altitude (a), and Rayleigh and FV3GFS winds at ~16.5 km altitude (b) in descending orbits. The TLS analysis line (green), the OLS regression line of FV3GFS winds on Aeolus winds (purple), and the OLS regression line of Aeolus winds on FV3GFS winds (transformed and plotted as a function of Aeolus winds in red) are shown, with corresponding regression coefficients displayed above each panel.

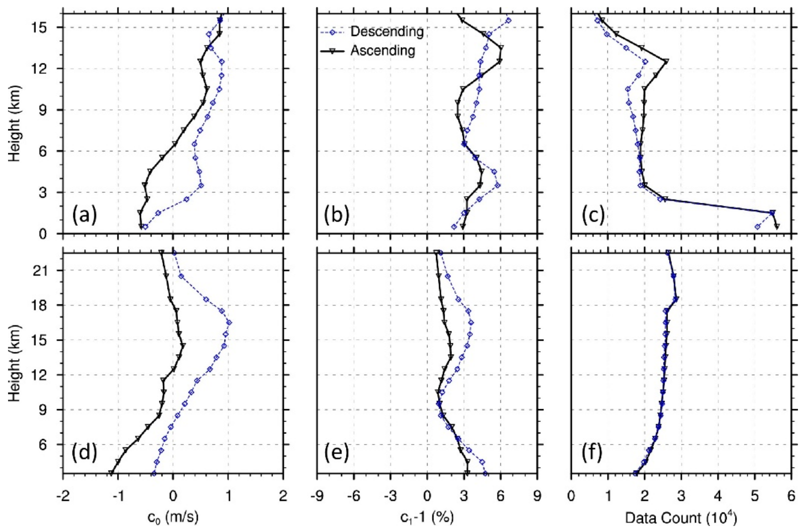

Figure 7. Vertical variations of TLS bias coefficients for Mie versus FV3GFS winds (a, b, c), and Rayleigh versus FV3GFS winds (d, e, f). Each point plotted represents a separate TLS analysis for all observations in each layer for all latitudes and for either ascending (black) or descending (blue) orbits. The symbols are plotted at the average height of the observations in each layer.

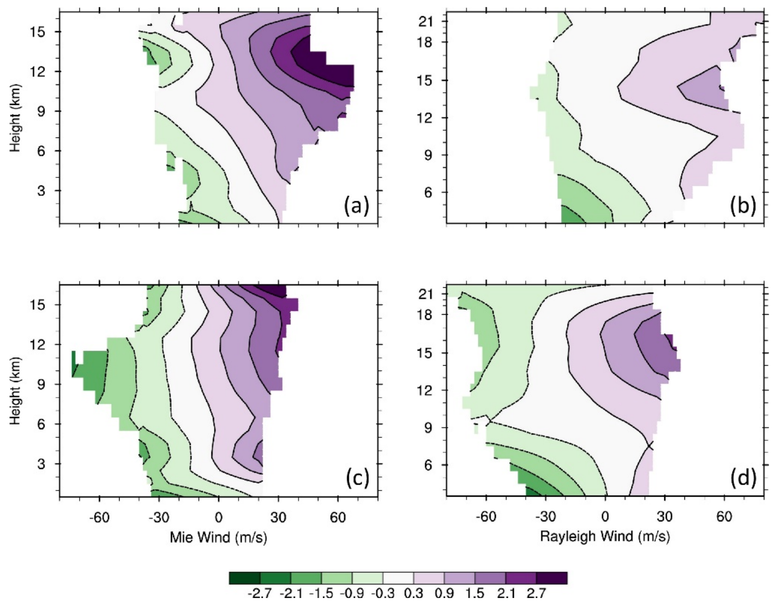

Figure 8. Vertical distributions of average TLS estimated biases (color scale, m/s) for Mie versus FV3GFS winds (a, c) and Rayleigh versus FV3GFS winds (b, d) as a function of observed Aeolus winds (m/s) in ascending (a, b) and descending (c, d) orbits for all latitudes, obtained from the TLS fits displayed in Figure 7.

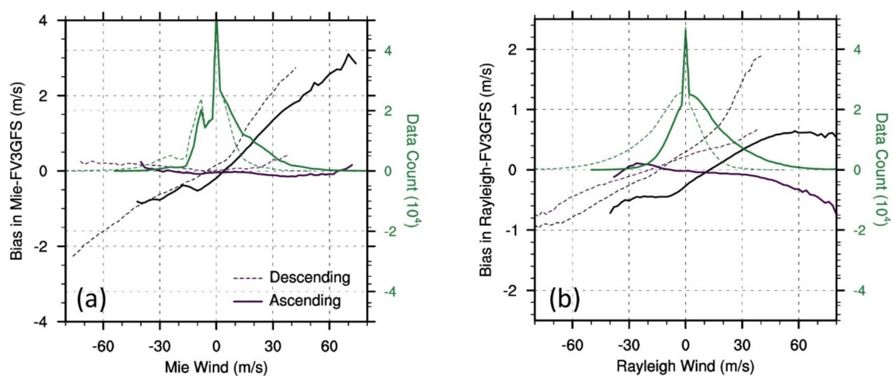

Figure 9. TLS estimated biases (m/s) before (black lines) and after (purple lines) TLS bias correction for Mie versus FV3GFS winds (a) and Rayleigh versus FV3GFS winds (b) as a function of the observed

https://doi.org/10.5194/amt-2022-20
Preprint. Discussion started: 18 January 2022
© Author(s) 2022. CC BY 4.0 License.
Atmospheric Measurement Techniques Discussions

Aeolus winds (m/s), vertically averaged for all latitudes of Aeolus winds. The green lines report the number of observations in each 2 m/s bin.

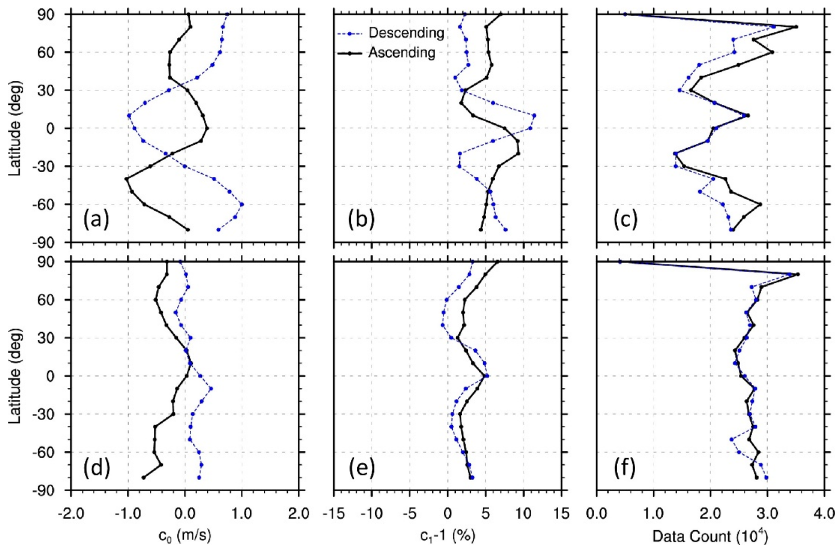

Figure 10. Latitudinal variation of TLS bias coefficients for Mie versus FV3GFS winds (a, b, c) and for Rayleigh versus FV3GFS winds (d, e, f). Each point plotted represents a separate TLS analysis for all observations in all vertical layers in a 10º latitude band for either ascending (black) or descending (blue) orbits. The latitude bands are centered every 10º from 90°S to 90°N. The symbols are plotted at the center in each latitude band. The vertical layers are 0-16 km for Mie winds and 3-22 km for Rayleigh winds.

https://doi.org/10.5194/amt-2022-20
Preprint. Discussion started: 18 January 2022
© Author(s) 2022. CC BY 4.0 License.
Atmospheric Measurement Techniques
Discussions

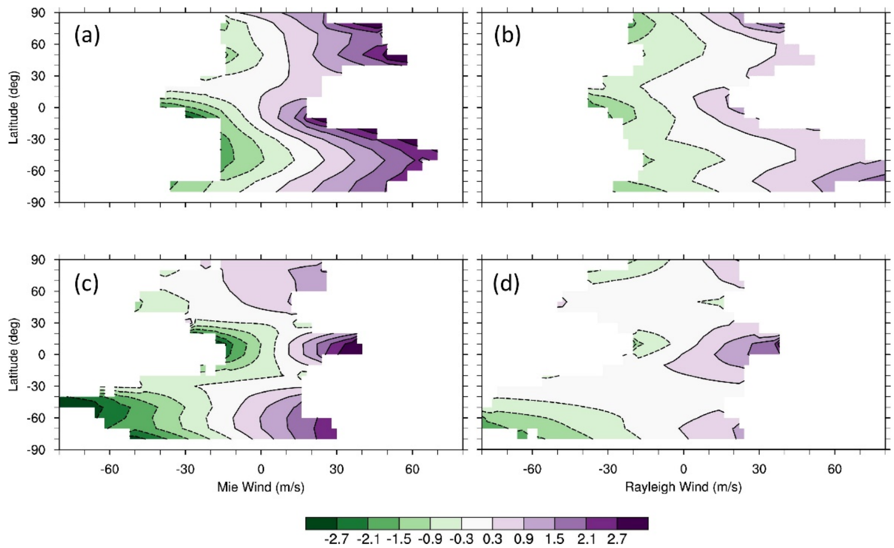

Figure 11. Latitudinal distributions of average TLS estimated biases (color scale, m/s) for Mie versus FV3GFS winds (a, c) and Rayleigh versus FV3GFS winds (b, d) as a function of Aeolus wind in ascending (a, b) and descending (c, d) orbits for all latitudes, obtained from the TLS fits displayed in Figure 10.

https://doi.org/10.5194/amt-2022-20
Preprint. Discussion started: 18 January 2022
© Author(s) 2022. CC BY 4.0 License.

Atmospheric Measurement Techniques Discussions

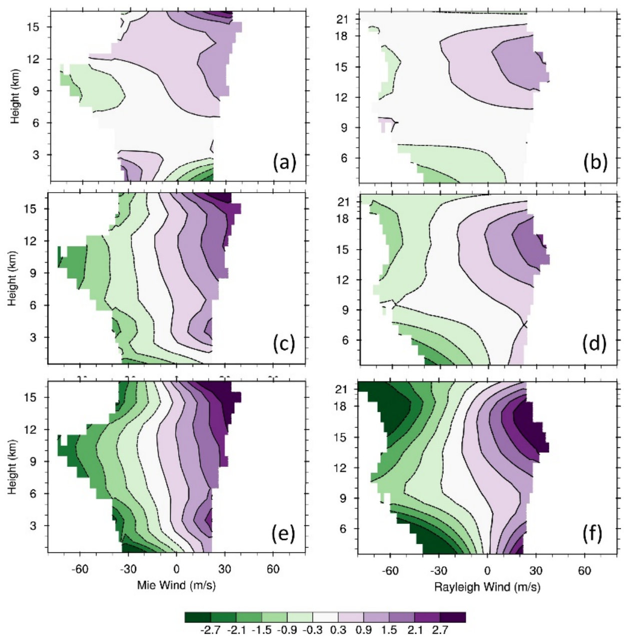

Figure 12. Vertical distributions of average bias estimates (color scale, m/s) in Mie versus FV3GFS winds (a, c, e) and Rayleigh versus FV3GFS winds (b, d, f) as a function of Aeolus winds using one of three methods for descending orbits for all latitudes. The methods are OLS using FV3GFS winds as a predictor (a, b), TLS (c, d, same as the bottom panels of Figure 8), and OLS using the average of Aeolus and FV3GFS as a predictor (e, f).

https://doi.org/10.5194/amt-2022-20
Preprint. Discussion started: 18 January 2022
© Author(s) 2022. CC BY 4.0 License.

482 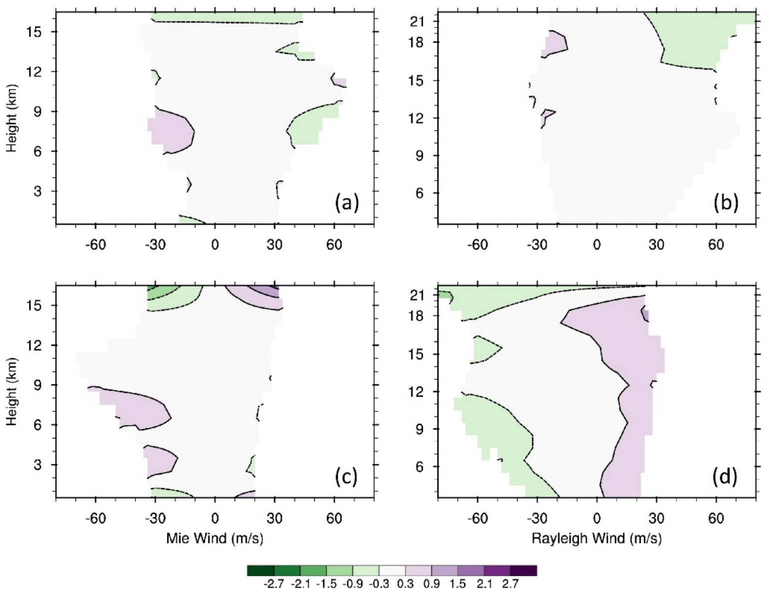

483 Figure 13. As in Figure 8 but for the mean innovation (O-B) after the TLS bias correction is applied. For
484 each 6-h cycle during 1-7 September 2019, the TLS bias correction is calculated from the 28 preceding
485 cycles.

486

https://doi.org/10.5194/amt-2022-20
Preprint. Discussion started: 18 January 2022
© Author(s) 2022. CC BY 4.0 License.
Atmospheric Measurement Techniques
Discussions

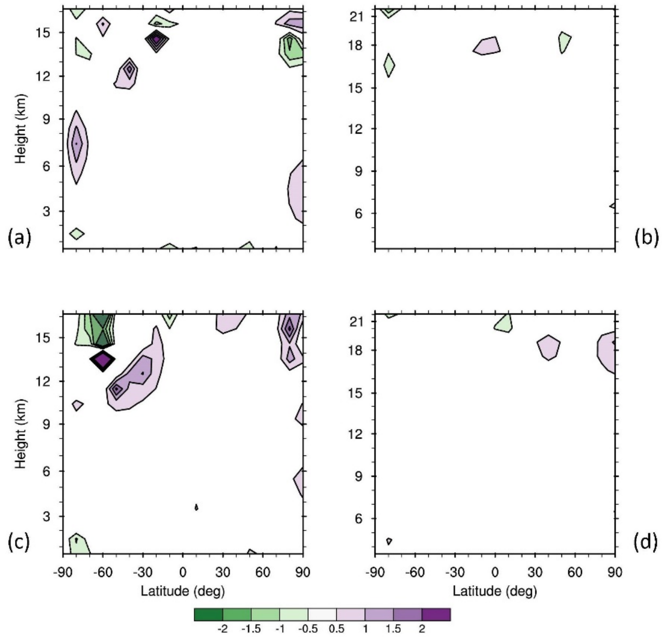

Figure 14. As in Figure 4 but after the TLS bias correction is applied. Note that the remaining bias in several bins are due to small sample size, and the TLS bias correction is not applied in these bins in Aeolus wind assimilation.